IOP Publishing New J. Phys. 27 (2025) 074301 https://doi.org/10.1088/1367-2630/ade61c

New Journal of Physics
The open access journal at the forefront of physics

Deutsche Physikalische Gesellschaft DPG
IOP Institute of Physics

Published in partnership with: Deutsche Physikalische Gesellschaft and the Institute of Physics

OPEN ACCESS

RECEIVED
9 February 2025

REVISED
10 June 2025

ACCEPTED FOR PUBLICATION
19 June 2025

PUBLISHED
9 July 2025

PAPER

Photon-polarization-resolved linear Breit–Wheeler pair production in a laser-plasma system

Huai-Hang Song[1,2,*] and **Zheng-Ming Sheng**[1,2,3]

[1] Key Laboratory for Laser Plasmas (MOE) and School of Physics and Astronomy, Shanghai Jiao Tong University, Shanghai 200240, People's Republic of China
[2] Collaborative Innovation Center of IFSA, Shanghai Jiao Tong University, Shanghai 200240, People's Republic of China
[3] Tsung-Dao Lee Institute, Shanghai Jiao Tong University, Shanghai 201210, People's Republic of China
[*] Author to whom any correspondence should be addressed.

E-mail: huaihangsong@sjtu.edu.cn

Keywords: laser-plasma interaction, linear Breit–Wheeler pair production, photon polarization, particle-in-cell simulation

Abstract

The linear Breit–Wheeler (LBW) process—the production of an electron–positron pair through the collision of two high-energy photons—can emerge as the dominant pair production mechanism in the ultraintense laser-plasma interaction for laser intensities below 10^{23} W cm^{-2}. Here, we explore the role of γ photon polarization in LBW pair production for a 10 PW-class, linearly polarized laser interacting with a solid-density plasma. The motivation for this investigation lies in two main aspects: γ photons emitted via nonlinear Compton scattering are inherently linearly polarized, and the LBW process exhibits a distinct sensitivity to γ photon polarization. By leveraging particle-in-cell simulations that self-consistently incorporate photon-polarization-resolved LBW pair production, our results reveal that γ photon polarization leads to a 5% to 10% reduction in the total LBW positron yield. This suppression arises because the polarization directions of the colliding γ photons are primarily parallel, reducing the LBW cross section compared to the unpolarized case. The influence of γ photon polarization weakens as the laser intensity increases or the scale length of preplasmas at the front of the target increases.

1. Introduction

The linear Breit–Wheeler (LBW) process describes electron–positron ($e^{\pm}$) pair production through the collision of two high-energy photons ($\gamma+\gamma\rightarrow e^{\pm}$) [1]. The condition for LBW pair production to occur is that the total energy of two colliding photons in the center-of-momentum (CM) frame—where the net momentum of two photons is zero—must exceed twice the rest mass energy of the electron $2m_ec^2\approx$ 1.02 MeV, where m_e is the electron mass and c is the speed of light in vacuum. Besides, the involved photons must be sufficiently dense to produce a significant number of $e^{\pm}$ pairs, as the maximum of the LBW cross section is just on the order of 10^{-25} cm^2. The long-standing absence of high-energy and dense photon sources has hindered the experimental observation of LBW pair production directly using real photons, although another form of it using intermediate photons has been experimentally confirmed [2].

The development of high-power laser facilities in PW and 10 PW classes [3–5] has opened unprecedented opportunities to investigate strong-field quantum electrodynamics (QED). The strong-field or nonlinear QED strength is primarily characterized by a parameter $\chi_e=\frac{e\hbar}{m_e^3c^4}|F_{\mu\nu}p^{\nu}|$, where $F_{\mu\nu}$ is the electromagnetic field tensor, p^{ν} is the electron four-momentum, e is the elementary charge, and $\hbar$ is the reduced Planck constant. The energetic electron can lose a significant portion of its energy by emitting individual γ photons via nonlinear Compton scattering ($e+n\omega_0\rightarrow e'+\gamma$) [6, 7]. Enhancing χ_e is typically achieved by colliding a laser pulse with a preaccelerated GeV-level electron beam, as is done in the laser-beam setup [8]. The emitted γ photons are high-energy, which is beneficial for the nonlinear Breit–Wheeler process (NBW, the production of an $e^{\pm}$ pair by a γ photon in the laser field, i.e. $\gamma+n\omega_0\rightarrow e^{\pm}$) [9–12]. However, the low density of γ photons is not conducive to the LBW process.

Alternatively, the plasma serves as an efficient medium that facilitates the significant conversion of laser photons into dense γ photons [13–19]. Previous studies on $e^{\pm}$ pair production in laser-plasma systems have primarily focused on the NBW process, which requires significantly higher laser intensities [13, 14]. For laser intensities below 10^{23} W cm^{-2} that are currently achievable [20], the LBW process becomes dominant and thus warrants particular attention. The use of laser-plasma-driven γ photons to probe LBW signals has garnered considerable attention [21–26]. A conventional laser-solid setup has been proposed recently to explicitly distinguish LBW pairs from other underlying mechanisms [27], which greatly simplifies experimental challenges. In addition to validating this fundamental QED process, generating quasimonoenergetic positrons seeded by the LBW process also provides new insights for positron applications [27, 28].

To more accurately predict LBW pair production in the laser-plasma interaction, it is essential to consider γ photon polarization for two reasons. First, γ photons emitted via nonlinear Compton scattering in the strong-field QED regime exhibit a high degree of linear polarization, with polarization degrees surpassing 50% [29–32]. Second, the LBW cross section depends on the polarization of the colliding γ photons, which affects the positron yield and positron emission direction [1, 33–35]. In astrophysics, for example, neglecting the polarization of synchrotron-radiated photons can lead to an overestimation of the $\gamma\gamma$ opacity by approximately 10% [36]. In laser-plasma systems, this issue remains unresolved as it has only recently become possible to self-consistently simulate polarized nonlinear Compton scattering [30–32] and unpolarized LBW pair production [26, 27] by modern particle-in-cell (PIC) simulations.

In this paper, we introduce how to implement the photon-polarization-resolved LBW process into a PIC code. Based upon this, we investigate the effect of γ photon polarization on LBW pair production in the interaction of a 10 PW-class, linearly polarized laser with a solid-density plasma. In the laser-solid interaction, electrons are accelerated by the laser fields to hundreds of MeV, and subsequently emit γ photons via nonlinear Compton scattering. The emitted γ photons exhibit high densities-comparable to that of solid electrons, 10^{23} cm^{-3}-and their poor collimation creates favorable conditions for $\gamma\gamma$ collisions, thereby facilitating the LBW process. We find that γ photon polarization reduces the total LBW positron yield by 5%–10% compared to the unpolarized case. This reduction arises because γ photons emitted via nonlinear Compton scattering are primarily linearly polarized within the laser polarization plane. After transforming to the CM frame, the polarization directions of the colliding γ photons are mostly parallel, leading to a smaller LBW cross section compared with the unpolarized one. The suppression due to γ photon polarization is angle-dependent, with a stronger effect on positrons emitted in directions perpendicular to the laser polarization plane. As the laser intensity increases, the γ photon energy rises while γ photon polarization decreases, both of which result in a diminished effect of γ photon polarization on LBW positrons.

The rest of this article is organized as follows. Section 2 introduces the theory and numerical method related to γ photon polarization in nonlinear Compton scattering and LBW pair production. In section 3, we present our PIC setup and simulation results for a solid-density plasma irradiated by a 10 PW-class linearly polarized laser, with a particular focus on polarization of emitted γ photons and its effect on LBW positrons. Section 4 provides a brief summary.

2. Two photon-polarization-resolved QED processes

2.1. Photon-polarization-resolved nonlinear Compton scattering

For unpolarized electrons, the polarization matrix of nonlinear Compton scattering probability under the locally constant field approximation is given by [37]

$$\frac{\mathrm{d}^2 W_{12}}{\mathrm{d}u\mathrm{d}t} = \frac{\mathrm{d}^2 W_{21}}{\mathrm{d}u\mathrm{d}t} = 0, \tag{1}$$

$$\frac{\mathrm{d}^2 W_{11}}{\mathrm{d}u\mathrm{d}t} = \frac{\alpha m_e^2 c^4}{2\sqrt{3}\pi\hbar\varepsilon_e}\left[\frac{u^2-2u+2}{1-u}K_{2/3}(\kappa) - \mathrm{Int}K_{1/3}(\kappa) + K_{2/3}(\kappa)\right], \tag{2}$$

$$\frac{\mathrm{d}^2 W_{22}}{\mathrm{d}u\mathrm{d}t} = \frac{\alpha m_e^2 c^4}{2\sqrt{3}\pi\hbar\varepsilon_e}\left[\frac{u^2-2u+2}{1-u}K_{2/3}(\kappa) - \mathrm{Int}K_{1/3}(\kappa) - K_{2/3}(\kappa)\right], \tag{3}$$

where $\alpha \approx 1/137$ is the fine structure constant, $K_{1/3}(\kappa)$ and $K_{2/3}(\kappa)$ are two modified Bessel functions of the second kind, $\mathrm{Int}K_{1/3}(\kappa) \equiv \int_{\kappa}^{\infty} K_{1/3}(x)\mathrm{d}x$, $\kappa = 2u/[3(1-u)\chi_e]$, $u = \varepsilon_\gamma/\varepsilon_e$, ε_γ is the γ photon energy, and ε_e is the electron energy before photon emission. Equations (2) and (3) are only valid in the interval of $0 < u < 1$ as ε_γ cannot exceed ε_e.

The polarization of γ photons is characterized by the Stokes vector $\boldsymbol{\xi} = (\xi_1, \xi_2, \xi_3)$ in the orthogonal basis of $(\hat{\boldsymbol{e}}_1, \hat{\boldsymbol{e}}_2, \hat{\boldsymbol{e}}_v)$ [37, 38], where $\hat{\boldsymbol{e}}_v$ is the velocity direction of the emitting electron, $\hat{\boldsymbol{e}}_1$ is its transverse

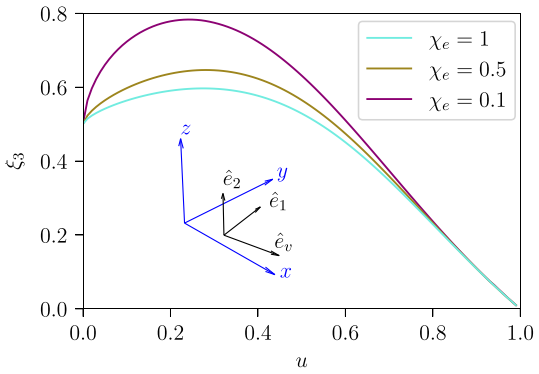

Figure 1. The photon polarization ξ_3, as a function of the photon energy ratio $u = \varepsilon_\gamma/\varepsilon_e$, is plotted according to equation (6) for three different QED parameters, $\chi_e = 0.1$, 0.5, and 1. The inset illustrates the Stokes basis ($\hat{\boldsymbol{e}}_1$, $\hat{\boldsymbol{e}}_2$, $\hat{\boldsymbol{e}}_v$), with the laser field linearly polarized in the x–y plane.

acceleration direction, and $\hat{\boldsymbol{e}}_2 = \hat{\boldsymbol{e}}_v \times \hat{\boldsymbol{e}}_1$. In our numerical module, the emission direction of γ photons is assumed to be collinear with the electron velocity. To simplify notation, we also use $\hat{\boldsymbol{e}}_v$ to represent the γ photon velocity. The ξ_1 and ξ_2 components are zero, leaving only the ξ_3 component [37],

$$\xi_1 = \frac{\mathrm{d}W_{12} + \mathrm{d}W_{21}}{\mathrm{d}W_{11} + \mathrm{d}W_{22}} = 0, \tag{4}$$

$$\xi_2 = \frac{i(\mathrm{d}W_{12} - \mathrm{d}W_{21})}{\mathrm{d}W_{11} + \mathrm{d}W_{22}} = 0, \tag{5}$$

$$\xi_3 = \frac{\mathrm{d}W_{11} - \mathrm{d}W_{22}}{\mathrm{d}W_{11} + \mathrm{d}W_{22}} = \frac{K_{2/3}(\kappa)}{\frac{u^2-2u+2}{1-u}K_{2/3}(\kappa) - \mathrm{Int}K_{1/3}(\kappa)}. \tag{6}$$

For simplicity of expression, we denote the third Stokes parameter ξ_3 as the photon polarization.

The mixed polarization state $|\xi_3| \leqslant 1$ represents the mean polarization of an ensemble of many real photons, or a macrophoton [38], which aligns with the PIC method. Unless otherwise specified, the term 'photon' in our simulation refers to this macrophoton. In particular, a γ photon with polarization ξ_3 means that a fraction of $(1+\xi_3)/2$ of real γ photons are linearly polarized along $\hat{\boldsymbol{e}}_1$, while a fraction of $(1-\xi_3)/2$ are polarized along $\hat{\boldsymbol{e}}_2$. Thus, the sign of ξ_3 determines the predominant orientation of γ photon polarization.

In principle, the Stokes bases for each γ photon are different, so they cannot be directly compared. However, for the linearly polarized laser field we focus on, the vectors $\hat{\boldsymbol{e}}_1$ and $\hat{\boldsymbol{e}}_v$ of γ photons lie within the laser polarization plane, which holds strictly in the one-dimensional (1D) setup and two-dimensional (2D) PIC setup with the p-polarized laser incidence. Here, we consider a laser linearly polarized in the x–y plane, consistent with the configuration adopted in section 3.1. Under the action of the laser field, electrons move within the laser polarization plane/simulation plane, i.e. the x–y plane. The transverse acceleration direction $\hat{\boldsymbol{e}}_1$ of the electrons is also parallel to the x–y plane, so $\hat{\boldsymbol{e}}_2 = \hat{\boldsymbol{e}}_v \times \hat{\boldsymbol{e}}_1$ is directed along the z-axis, as illustrated in the inset of figure 1. As a result, γ photon polarization ξ_3 in the linearly polarized laser field can be interpreted as follows: $(1+\xi_3)/2$ of real γ photons are linearly polarized parallel to the laser polarization plane, denoted as $\gamma_\parallel$ photons, and $(1-\xi_3)/2$ are linearly polarized perpendicular to the laser polarization plane, denoted as $\gamma_\perp$ photons.

Equation (6) is visualized in figure 1 for three different QED parameters: $\chi_e = 0.1$, 0.5, and 1. It shows that emitted γ photons are highly linearly polarized, with the average photon polarization $\xi_3 > 0$, indicating that γ photons are primarily polarized along $\hat{\boldsymbol{e}}_1$. As the photon energy ratio $u = \varepsilon_\gamma/\varepsilon_e$ increases, ξ_3 rises from 50% at $u \to 0$, reaching a maximum of 0.6–0.8 at $u \approx 0.2$–0.4, and then decreases to 0 as $u \to 1$. Additionally, ξ_3 decreases with increasing χ_e at a given u, indicating that γ photon polarization weakens as χ_e, which is mainly determined by the laser intensity in laser-plasma interactions, increases.

2.2. Photon-polarization-resolved LBW pair production

In the pioneering work [1], Breit and Wheeler derived the LBW cross section for two types of pure linear polarization states. In the CM frame, the linear polarizations of two colliding photons are represented by ξ_3' and ξ_3'', with the primes distinguishing the first and second photon, respectively. The emission direction of the generated positron, $\hat{\boldsymbol{e}}_+$, is defined in terms of a polar angle θ (relative to the $\hat{\boldsymbol{e}}_v$ axis) and an azimuthal angle φ (in the plane spanned by $\hat{\boldsymbol{e}}_1$ and $\hat{\boldsymbol{e}}_2$), such that $\hat{\boldsymbol{e}}_+ = \cos\theta\,\hat{\boldsymbol{e}}_v + \sin\theta\cos\varphi\,\hat{\boldsymbol{e}}_1 + \sin\theta\sin\varphi\,\hat{\boldsymbol{e}}_2$ and the corresponding solid angle $\mathrm{d}\Omega = \sin\theta\mathrm{d}\theta\mathrm{d}\varphi$. The LBW cross sections for parallel photon polarization ($\xi_3' = 1$

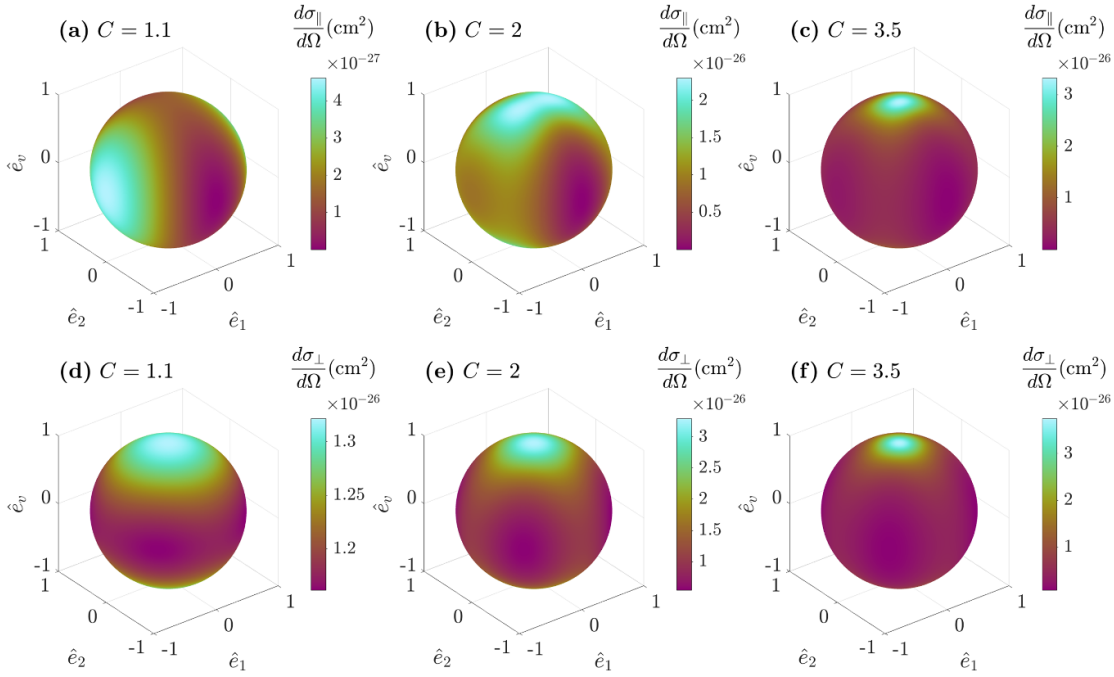

Figure 2. The theoretical LBW cross sections, with the positron emission angle resolved, for parallel γ photon polarization ((a)–(c), where both γ photons are linearly polarized along the $\hat{\boldsymbol{e}}_1$ direction) and perpendicular γ photon polarization ((d)–(f), with one γ photon linearly polarized along the $\hat{\boldsymbol{e}}_1$ direction and the other along the $\hat{\boldsymbol{e}}_2$ direction) are shown for three different CM photon energies $C = 1.1$ ((a), (d)), $C = 2$ ((b), (e)), and $C = 3.5$ ((c), (f)), as calculated using equations (7) and (8).

and $\xi_3'' = 1$) and perpendicular photon polarization ($\xi_3'\xi_3'' = -1$) are expressed as [1]

$$\frac{\mathrm{d}\sigma_\parallel}{\mathrm{d}\Omega}(\theta,\varphi) = \sigma_0\left[S^2 - 2S^2\left(N^2 - M^2\right) - S^4\left(N^2 - M^2\right)^2 + S^2C^2\left(1-\Lambda^2\right)\right], \tag{7}$$

$$\frac{\mathrm{d}\sigma_\perp}{\mathrm{d}\Omega}(\theta,\varphi) = \sigma_0\left[C^2 - 4S^4M^2N^2 + S^2C^2\left(1-\Lambda^2\right)\right], \tag{8}$$

where $\sigma_0 = r_e^2 S/[2C^3(C^2-\Lambda^2S^2)^2]$ and $r_e = e^2/m_ec^2 \approx 2.82\times10^{-13}$ cm is the classical electron radius. Here, $C \equiv \cosh\Theta$ is defined as the energy of one of the photons normalized to m_ec^2 in the CM frame—hereafter referred to as *CM photon energy*, and $S \equiv \sinh\Theta$. The cosine values of the angles between the positron emission direction $\hat{\boldsymbol{e}}_+$ and the vectors $\hat{\boldsymbol{e}}_1$, $\hat{\boldsymbol{e}}_2$, and $\hat{\boldsymbol{e}}_v$ are denoted by M, N, and Λ, respectively. Therefore, the relation $M^2 + N^2 + \Lambda^2 = 1$ holds.

According to equations (7) and (8), the LBW cross sections for two types of photon polarization at three different CM photon energies are illustrated in figures 2(a)–(f). For the low CM photon energy of $C = 1.1$, parallel photon polarization significantly affects the angular distribution of positron emission, with positrons being preferentially emitted along the photon polarization direction $\hat{\boldsymbol{e}}_1$ (figure 2(a)). In contrast, perpendicular photon polarization has a small effect on the positron emission direction for the small C, with positrons being emitted somewhat preferentially along the photon velocity direction (figure 2(d)). As the CM photon energy increases to $C = 3.5$, the polarization effect weakens, and positron emission becomes more concentrated along the photon velocity direction $\hat{\boldsymbol{e}}_v$ for both polarization types (figures 2(c) and (f)).

By summing over the positron emission angle θ and φ in equations (7) and (8), the total LBW cross sections for both parallel and perpendicular photon polarizations can be obtained [1]:

$$\sigma_\parallel = \frac{\pi r_e^2}{2}\left(4\Theta C^{-2} + 4\Theta C^{-4} - 3\Theta C^{-6} - 2SC^{-3} - 3SC^{-5}\right), \tag{9}$$

$$\sigma_\perp = \frac{\pi r_e^2}{2}\left(4\Theta C^{-2} + 4\Theta C^{-4} - \Theta C^{-6} - 2SC^{-3} - SC^{-5}\right). \tag{10}$$

In a linearly polarized laser field, equations (7)–(10) are readily generalized to partially polarized photons. The collision of two partially polarized photons with polarization ξ_3' and ξ_3'' involves four distinct classes of real photons according to whether their polarization is parallel or perpendicular to the laser polarization plane: $\gamma_\parallel'$, $\gamma_\perp'$, $\gamma_\parallel''$, and $\gamma_\perp''$. Following Lorentz transformation to the CM frame, $\gamma_\parallel'$ and $\gamma_\parallel''$ photons maintain parallel polarization [39], accounting for a fraction of $(1+\xi_3')(1+\xi_3'')/4$ of the total real

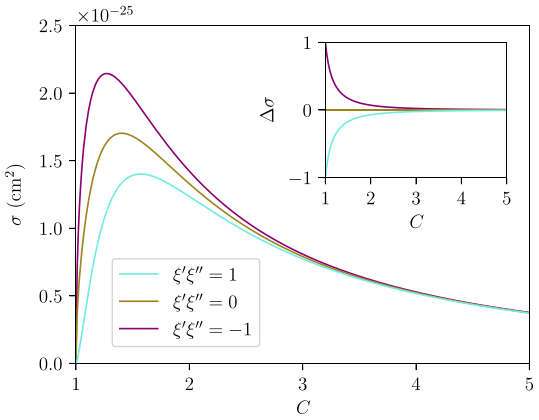

Figure 3. The total LBW cross section σ as a function of the CM photon energy C for parallel ($\xi_3'\xi_3'' = 1$), perpendicular ($\xi_3'\xi_3'' = -1$), and unpolarized ($\xi_3'\xi_3'' = 0$) photon polarizations, plotted based on equation (12). The relative deviation of the polarized cross section from the unpolarized result, $\Delta\sigma = (\sigma - \overline{\sigma})/\overline{\sigma}$, is shown in the inset.

photons. Similarly, $\gamma_\perp'$ and $\gamma_\perp''$ photons also preserve parallel polarization, contributing $(1-\xi_3')(1-\xi_3'')/4$. When one photon is polarized parallel to the laser polarization plane and the other perpendicular, such as $\gamma_\parallel'$ and $\gamma_\perp''$ photons, or $\gamma_\perp'$ and $\gamma_\parallel''$ photons, their mutual perpendicular polarization persists in the CM frame, contributing fractions $(1+\xi_3')(1-\xi_3'')/4$ and $(1-\xi_3')(1+\xi_3'')/4$, respectively. Finally, the LBW cross section, with positron emission angle and photon polarization resolved, is formulated as

$$\begin{aligned}\frac{\mathrm{d}\sigma}{\mathrm{d}\Omega}(\theta,\varphi) = &\frac{1+\xi_3'}{2}\frac{1+\xi_3''}{2}\times\frac{\mathrm{d}\sigma_\parallel}{\mathrm{d}\Omega}(\theta,\varphi) + \frac{1-\xi_3'}{2}\frac{1-\xi_3''}{2}\times\frac{\mathrm{d}\sigma_\parallel}{\mathrm{d}\Omega}(\theta,\varphi+\pi/2)\\ &+\left[\frac{1+\xi_3'}{2}\frac{1-\xi_3''}{2}+\frac{1-\xi_3'}{2}\frac{1+\xi_3''}{2}\right]\times\frac{\mathrm{d}\sigma_\perp}{\mathrm{d}\Omega}(\theta,\varphi).\end{aligned} \tag{11}$$

Similarly, the photon-polarization-resolved total LBW cross section is written as

$$\begin{aligned}\sigma &= \left(\frac{1+\xi_3'}{2}\frac{1+\xi_3''}{2}+\frac{1-\xi_3'}{2}\frac{1-\xi_3''}{2}\right)\times\sigma_\parallel + \left(\frac{1+\xi_3'}{2}\frac{1-\xi_3''}{2}+\frac{1-\xi_3'}{2}\frac{1+\xi_3''}{2}\right)\times\sigma_\perp\\ &= \frac{\pi r_e^2}{2}\left[4\Theta C^{-2}+4\Theta C^{-4}-(2+\xi_3'\xi_3'')\Theta C^{-6}-2SC^{-3}-(2+\xi_3'\xi_3'')SC^{-5}\right].\end{aligned} \tag{12}$$

Using the two basic mathematical identities $C^2 - S^2 = 1$ and $\Theta = \ln\left(C+\sqrt{C^2-1}\right)$, the photon-polarization-averaged total LBW cross section $\overline{\sigma}$ can be expressed into a commonly used form [40]:

$$\overline{\sigma} = \frac{\pi r_e^2}{2}\left(1-\nu^2\right)\left[2\nu^3 - 4\nu + \left(3-\nu^4\right)\ln\left(\frac{1+\nu}{1-\nu}\right)\right], \tag{13}$$

where $\nu = \sqrt{1-1/C^2}$.

Figure 3 shows the total LBW cross sections, calculated using equation (12), for parallel, perpendicular, and unpolarized photon polarizations. Parallel polarization results in a reduced cross section compared to the unpolarized case at the same CM photon energy C. In contrast, perpendicular polarization increases the cross section. For both parallel and perpendicular polarizations, the modulus of relative variation between the polarized and unpolarized results, $\Delta\sigma = (\sigma - \overline{\sigma})/\overline{\sigma}$, decreases from 100% at $C \to 1$ to 0 as $C \gg 1$. Therefore, the polarization effect on LBW pair production is most pronounced by relatively low-energy photons.

The normalized CM photon energy C must be greater than 1 for LBW pair production. In the laboratory frame, this implies that the product of two photon energies $\varepsilon_1\varepsilon_2$ must be greater than $2m_e^2c^4/(1-\cos\theta_{12})$, where θ_{12} is the intersecting angle between two photons. Given that the energy of a laser photon is only about 1 eV, the threshold energy required for the other photon is about 1 TeV. However, the maximum energy of emitted γ photons in laser-plasma interactions typically reaches only the sub-GeV level. Therefore, laser photons cannot produce $e^\pm$ pairs by colliding with γ photons via the LBW process. Two involved photons are both the emitted γ photons.

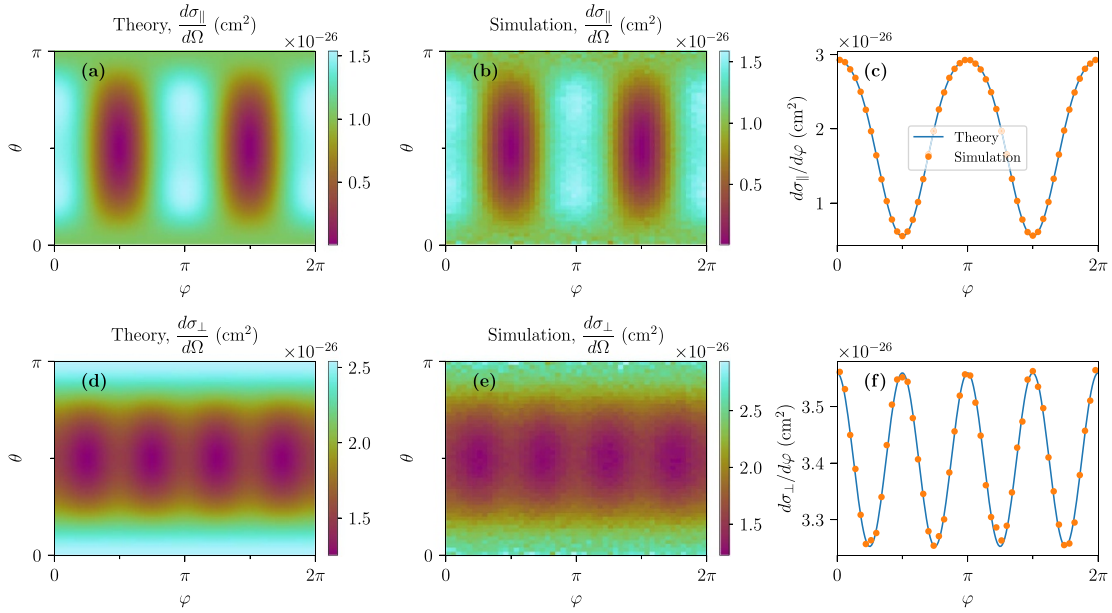

Figure 4. The comparison of LBW cross sections between theories and simulations, with the positron emission angle resolved, for parallel ((a)–(c)) and perpendicular ((d)–(f)) photon polarizations.

2.3. PIC implementation

The photon-polarization-resolved nonlinear Compton scattering has been implemented into the YUNIC PIC code [41] in our previous works [31, 42]. Here, we introduce how to implement photon-polarization-resolved LBW pair production into the 1D/2D PIC code using the Monte-Carlo sampling based on equation (11).

For the linearly polarized laser field in the 1D setup or the 2D setup with the p-polarized laser incidence, the motion of electrons and γ photons is confined to the laser polarization plane. Therefore, the polarization ξ_3 of emitted γ photons calculated via equation (6) can be directly inserted into equation (11) without the need for additional transformation, according to section 2.2. Specifically, three uniform random numbers U_1, U_2 and U_3 between 0 and 1 are required to determine if an $e^\pm$ pair is generated after the collision of γ photons and its possible angular distribution. The polar and azimuthal angles of the generated positron are sampled by $\theta = U_1 \times \pi$ and $\varphi = U_2 \times 2\pi$. If the pair production probability $P_{\rm LBW} = \pi \times 2\pi \times \mathbb{F}_{\rm mult}\mathbb{N}_{\rm ratio}{\rm Max}(w_1, w_2)\frac{d\sigma}{d\Omega}(\theta,\varphi)$ $(1-\cos\theta_{12})c\Delta t/\Delta V$ is greater than U_3, then an $e^\pm$ pair with the weight of ${\rm Min}(w_1, w_2)/\mathbb{F}_{\rm mult}$ is created; otherwise, pair production is rejected. Here, $w_{1,2}$ denotes the weight of two colliding γ photons, Δt the PIC time step, ΔV the PIC cell volume, $\mathbb{N}_{\rm ratio}$ is to compensate for not making all possible pairings for efficiency, and $\mathbb{F}_{\rm mult}$ is the multiplication factor that actually does not affect the positron yield. The pairwise collision of γ photons with different weights was detailed in [26], including the functional roles of two factors $\mathbb{N}_{\rm ratio}$ and $\mathbb{F}_{\rm mult}$ [43].

We benchmark our photon-polarization-resolved LBW algorithm through simulating the collision between two linearly polarized γ photon beams using the 1D version of the YUNIC code. The simulation is performed in a 10 μm domain discretized into 320 uniform grid cells. Periodic boundary conditions are applied for both fields and particles. Two monoenergetic γ photon beams, each with an uniform density of $1.1 \times 10^{24}\,{\rm cm}^{-3}$ and an energy of 1.3 MeV, collide head-on. Figures 4(a)–(f) show the angular number distribution of generated positrons for parallel and perpendicular photon polarizations. Quantitative comparison reveals that our simulation results demonstrate excellent agreement with theoretical predictions for both polarization types.

3. Simulation parameters and results

3.1. Simulation setup

To investigate the effect of γ photon polarization on LBW pair production in the laser-plasma interaction, we perform PIC simulations using the 2D version of the YUNIC code. We model a thick, fully ionized solid carbon target, with the target's front positioned at $x = 10\,\mu$m and its rear extending to the right boundary of the simulation domain. The electron density of the bulk plasma is set to $200n_c$, where $n_c = m_e\omega_0^2/4\pi e^2$ is the critical plasma density and ω_0 is the laser angular frequency. To account for laser prepulses in real

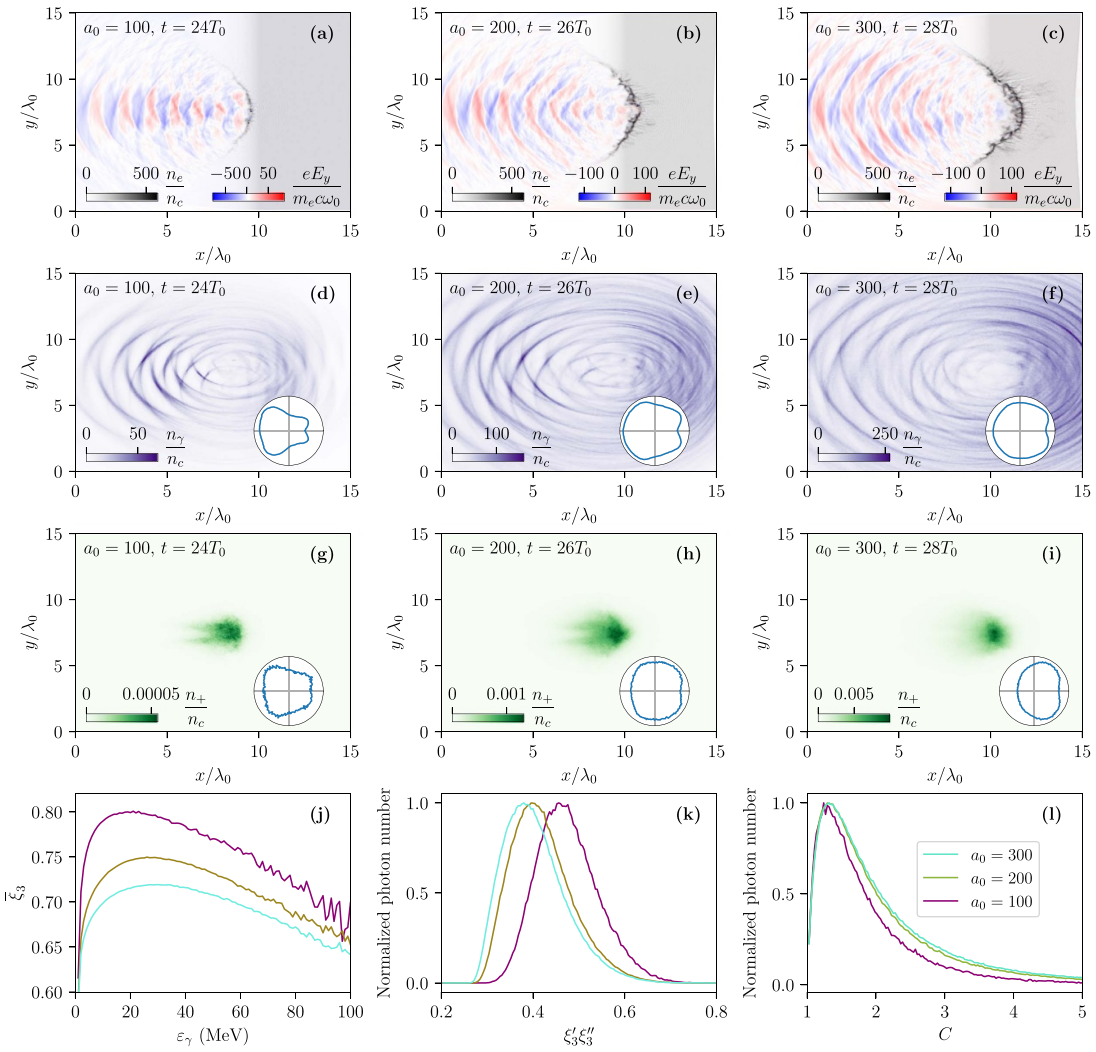

Figure 5. PIC simulation results for three laser intensities at the end of the interaction ($t = 24T_0$ for $a_0 = 100$ (a), (d), (g), $t = 26T_0$ for $a_0 = 200$ (b), (e), (h), and $t = 28T_0$ for $a_0 = 300$ (c), (f), (i)). (a)–(i) Snapshots of the laser electric field E_y, together with the electron density n_e ((a)–(c)), γ photon density n_γ with the photon energy greater than $0.1m_ec^2$ ((d)–(f)), and positron density n_+ (positron motion is ignored) ((g)–(i)), where γ photon polarization is included. The inserts in (d)–(i) show the corresponding angular number distribution in the x–y plane. (j) The average γ photon polarization $\bar{\xi}_3$ as a function of the photon energy ε_γ. The normalized number distribution of annihilated γ photons as a function of the polarization product $\xi_3'\xi_3''$ and CM photon energy C is displayed in (k) and (l), respectively.

experiments, a low-density preplasma with an exponential scale length of $L_0 = 1\,\mu$m is assumed at the target's front. A laser pulse, linearly polarized along the y direction, is normally incident from the left boundary onto the target. The laser has a central wavelength of $\lambda_0 = 1\,\mu$m, a normalized amplitude $a_0 = eE_0/m_ec\omega_0 = 100$–$300$, a FWHM duration of $5T_0$ ($T_0 = \lambda_0/c \approx 3.3$ fs), and a waist radius of $3\lambda_0$. The simulation domain in the x–y plane is set to $L_x \times L_y = 15\,\mu\text{m} \times 15\,\mu$m, with a resolution of 480×480 cells. The number of ions per cell is fixed at 36, while the number of electrons per cell depends on the laser intensity: 400 for $a_0 = 100$, 225 for $a_0 = 200$, and 100 for $a_0 = 300$. The increased number of electrons per cell at lower laser intensities is aimed at improving the statistical accuracy of generated LBW pairs. Absorbing boundaries are applied for both fields and particles in each direction. Only photons with energy exceeding $0.1m_ec^2$ are saved in our simulations. Based on our recent work [26] using similar parameters, the LBW process dominates over the NBW process for normalized laser amplitudes $a_0 < 400$–500 as the NBW process is exponentially suppressed in the weak field. Thus, only the LBW process is discussed here.

3.2. Simulation results

Figures 5(a)–(i) display snapshots of the laser electric field, electron density, γ photon density and positron density at the end of the interaction for three different laser intensities. The positron density as shown in figures 5(g)–(i), less than $0.01n_c$ for $a_0 < 300$, is much lower than the target plasma density, indicating that the feedback from generated $e^\pm$ pairs on laser-plasma dynamics can be neglected. Since we focus on the

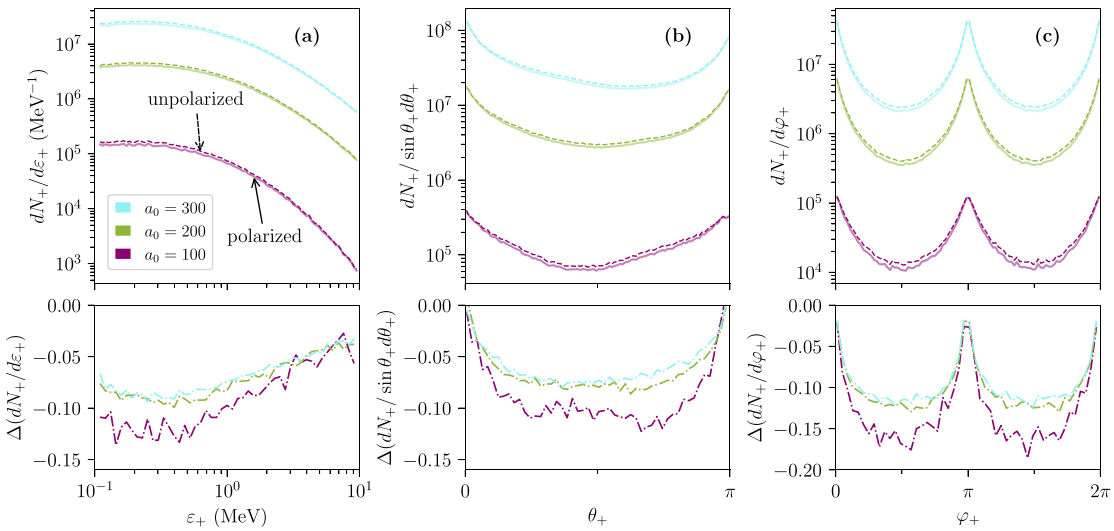

Figure 6. The positron number distributions as a function of the positron energy ε_+ (a), polar angle of positron emission θ_+ relative to the $+x$ axis (b), and azimuthal angle of positron emission φ_+ measured counterclockwise from the $+y$ axis with respect to $+x$ axis (c) for the polarized (solid) and unpolarized (dashed) cases, and their relative variations (dashed-dotted).

influence of γ photon polarization on LBW pair production, the subsequent motion of positrons after their creation is not considered. The corresponding angular number distribution of γ photons is shown in the insets of figures 5(d)–(f). Overall, γ photon emission in the laser-solid interaction is somewhat isotropic within the laser polarization plane. While this isotropy is unfavorable for the application of γ photons, it is highly beneficial for the LBW process, in which γ photon collisions are essential. More specifically, γ photon emission shifts from being predominantly backward-directed to forward-directed as the laser intensity increases from $a_0 = 100$ to 300. Similarly, the angular distribution of positron emission mirrors that of γ photons, as shown in the insets of figures 5(g)–(i).

Figure 5(j) illustrates that emitted γ photons are highly linearly polarized. The average γ photon polarization $\overline{\xi}_3 > 0$ indicates that linear polarization of emitted γ photons is predominantly parallel to the laser polarization plane. As the γ photon energy increases, $\overline{\xi}_3$ initially increases, reaching a peak of approximately 0.8, 0.75, and 0.72 for laser intensities $a_0 = 100$, 200, and 300, respectively. As the laser intensity increases, γ photon polarization decreases across the entire energy range, consistent with figure 1. The high polarization of emitted γ photons results in the polarization product $\xi_3'\xi_3'' > 0$ for LBW pair production, as both $\xi_3' > 0$ and $\xi_3'' > 0$ for two colliding γ photons. The normalized number distribution of annihilated γ photons as a function of the polarization product is shown in figure 5(k). The polarization product associated with the highest number of annihilated γ photons is approximately 0.45, 0.4, and 0.38 for $a_0 = 100$, 200, and 300, respectively. Another important parameter for assessing the impact of γ photon polarization is the CM photon energy. The CM energy of annihilated γ photons is primarily concentrated in the low-energy range, peaking at around $C = 1.3$ for all three laser intensities, as shown in figure 5(l). This is consistent with figure 3, which shows the LBW cross section is maximized at around $C = 1.3$.

The positive polarization product and low CM photon energy suggest that γ photon polarization will have a suppression impact on LBW pair production, according to figure 3. When γ photon polarization is taken into account, our PIC simulation results indicate that the total LBW positron yield is reduced by approximately 5%–10% compared to the unpolarized case. To reduce the uncertainty introduced by the Monte-Carlo method, the same random number seed is used in both the polarized and unpolarized simulations to ensure that the emitted γ photons and pairwise collisions are identical. With the increase of laser intensities, the modulus of relative variation in the total positron yield between the polarized and unpolarized cases, $|\Delta N_+|$, decreases from 9.7% at $a_0 = 100$ to 6.5% at $a_0 = 300$, with ΔN_+ defined as $(N_+^{\rm pol} - N_+^{\rm unpol})/N_+^{\rm unpol}$. There are two main reasons for this decrease: (i) the photon polarization product decreases (figure 5(k)); (ii) the CM photon energy increases (figure 5(l)). According to theoretical predictions shown in figure 3, both the increase of the CM photon energy and the decrease of the polarization product reduce the influence of γ photon polarization on the LBW cross section, which is consequently reflected in ΔN_+.

The suppression of positron production by γ photon polarization also depends on the positron energy and the positron emission direction. Figure 6(a) illustrates that the positron energy at the creation time is relatively low, as low-energy γ photons dominate in nonlinear Compton scattering. In agreement with

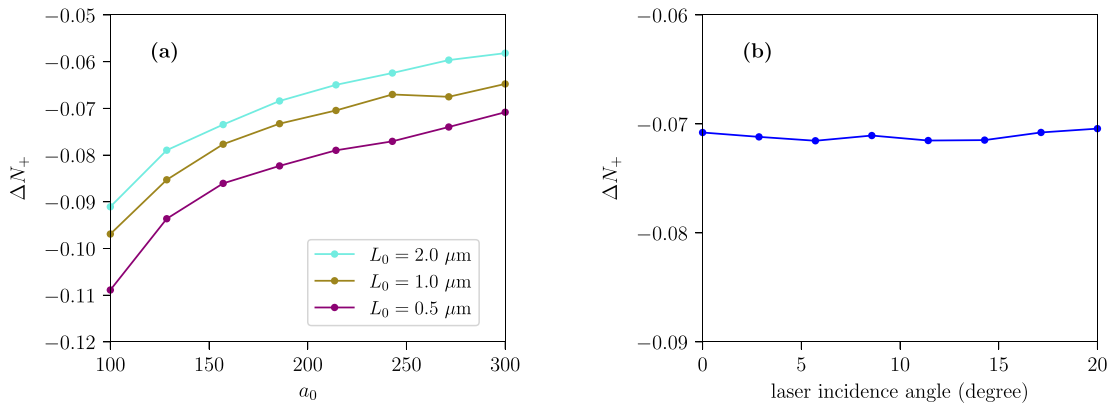

Figure 7. The relative variations in the total positron number between the polarized and unpolarized cases, ΔN_+, as a function of the laser intensity for different preplasma scale lengths at the normal laser incidence (a) and as a function of the laser incidence angle for $a_0 = 200$ and $L_0 = 1.0\ \mu$m (b).

figure 3, the impact of γ photon polarization on low-energy positrons is generally more significant than on high-energy positrons, i.e. $|\Delta(\mathrm{d}N_+/\mathrm{d}\varepsilon_+)|$ decreases as the positron energy increases. The influence of γ photon polarization on the positron number is most pronounced at $\theta_+ = \pi/2$ and $\varphi_+ = \pi \pm \pi/2$, as shown in figures 6(b) and (c). This indicates that γ photon polarization primarily affects positron emission in directions outside the laser polarization plane, while its effect within the laser polarization plane is relatively weak. This behavior can be explained by the theoretical LBW cross sections shown in figures 3(a) and (b) that positrons are predominantly emitted along the γ photon polarization direction for parallel γ photon polarization, which is parallel to the laser polarization plane. Therefore, the number of positrons emitted perpendicular to the laser polarization is significantly lower compared to the unpolarized case.

Figure 7(a) illustrates the suppression of the total positron yield by γ photon polarization for various laser intensities and preplasma scale lengths at the normal laser incidence. As the normalized laser amplitude a_0 increases, the modulus of relative suppression $|\Delta N_+|$ decreases across all preplasma scale lengths. For the shortest scale length ($L_0 = 0.5\ \mu$m), $|\Delta N_+|$ falls from about 0.11 at $a_0 = 100$ to roughly 0.07 at $a_0 = 300$. For the intermediate and long scale lengths ($L_0 = 1.0\ \mu$m and $2.0\ \mu$m), the suppression decreases from approximately 0.095 and 0.09 at $a_0 = 100$ to about 0.065 and 0.058 at $a_0 = 300$, respectively. This trend indicates that shorter preplasma scale lengths amplify the polarization-induced reduction in positron production. We have also examined the case of the p-polarized laser under the oblique incidence. The results shown in figure 7(b) indicate that for the incidence angle up to 20 degree, there is no significant difference compared to the normal incidence.

Finally, we would like to add three points. First, although our comparison shows that γ photon polarization reduces the LBW positron yield, this does not imply that the γ photon polarization effect can be directly verified in experiments. It is impossible to 'turn off' γ photon polarization in corresponding laser-solid experiments. Therefore, to experimentally verify the influence of γ photon polarization on the LBW process, a carefully designed experimental setup is required. Since the polarization of emitted γ photons depends on the polarization of the laser, at least two laser pulses may be required. By varying the relative polarization between the two laser pulses, one could control the polarization of the colliding γ photons. How to ensure that the γ photon density for the collision is not affected by the laser polarization may be a challenge. Second, the angle-dependent impact of γ photon polarization on positron production is observed at the moment of their creation. Once the subsequent influence of laser fields is considered, positrons will acquire significant momentum parallel to the laser polarization plane via laser acceleration [27], which will substantially disrupt this angular dependence. Therefore, in future laser-plasma experiments aimed at verifying the angle-dependent γ photon polarization effect on the LBW process, it will be crucial to minimize the influence of laser fields on generated positrons. Third, although we used 2D simulations, the γ photon energy spectrum in the 3D case agrees well with the 2D results when the laser waist radius exceeds 3 μm. Moreover, the γ photon emission remains well confined within the laser polarization plane. Therefore, our 2D results can reliably reflect the essential features of the realistic three-dimensional scenario.

4. Conclusion

We have investigated the impact of γ photon polarization on LBW pair production during the interaction of a linearly polarized laser with solid-density plasmas. The γ photons emitted via nonlinear Compton

scattering are predominantly linearly polarized parallel to the laser polarization plane, with a polarization degree exceeding 50%. During the collision of such polarized γ photons, parallel γ photon polarization dominates, resulting in a reduced LBW cross section relative to the unpolarized case. Our 2D PIC simulations reveal that γ photon polarization reduces the total LBW positron yield by 5%–10%. Additionally, increasing laser intensities reduces the suppression effect of γ photon polarization. Although we focus on the interaction between a laser and a solid-density plasma, the findings have implications for other laser-plasma systems as γ photons emitted through nonlinear Compton scattering are intrinsically linearly polarized.

Remarkably, when these results are combined with our previous investigations on NBW pair production [31, 42], it becomes clear that γ photon polarization suppresses both LBW and NBW processes by a similar extent (approximately 5%–10%) in linearly polarized laser-driven plasmas. Moreover, in both processes, the γ photon polarization effect weakens as the laser intensity increases.

Data availability statement

The data cannot be made publicly available upon publication because no suitable repository exists for hosting data in this field of study. The data that support the findings of this study are available upon reasonable request from the authors.

Acknowledgments

This work was supported by the National Natural Science Foundation of China (Grant Nos. 12405285 and 12135009) and the China Postdoctoral Science Foundation (Grant No. 2023M742294). The simulations were performed on the π 2.0 supercomputer at Shanghai Jiao Tong University.

References

[1] Breit G and Wheeler J A 1934 Collision of two light quanta *Phys. Rev.* **46** 1087–91
[2] Adam J *et al* 2021 Measurement of e^+e^- momentum and angular distributions from linearly polarized photon collisions *Phys. Rev. Lett.* **127** 052302
[3] Li A X *et al* 2022 Acceleration of 60 MeV proton beams in the commissioning experiment of the SULF-10 PW laser *High Power Laser Sci. Eng.* **10** e26
[4] Tanaka K A *et al* 2020 Current status and highlights of the ELI-NP research program *Matter Radiat. Extremes* **5** 024402
[5] Burdonov K *et al* 2021 Characterization and performance of the Apollon short-focal-area facility following its commissioning at 1 PW level *Matter Radiat. Extremes* **6** 064402
[6] Cole J M *et al* 2018 Experimental evidence of radiation reaction in the collision of a high-intensity laser pulse with a laser-wakefield accelerated electron beam *Phys. Rev. X* **8** 011020
[7] Poder K *et al* 2018 Experimental signatures of the quantum nature of radiation reaction in the field of an ultraintense laser *Phys. Rev. X* **8** 031004
[8] Blackburn T G 2020 Radiation reaction in electron-beam interactions with high-intensity lasers *Rev. Mod. Plasma Phys.* **4** 5
[9] Reiss H R 1962 Absorption of light by light *J. Math. Phys.* **3** 59–67
[10] Burke D L *et al* 1997 Positron production in multiphoton light-by-light scattering *Phys. Rev. Lett.* **79** 1626–9
[11] Di Piazza A 2016 Nonlinear Breit-Wheeler pair production in a tightly focused laser beam *Phys. Rev. Lett.* **117** 213201
[12] Blackburn T G, Ilderton A, Murphy C D and Marklund M 2017 Scaling laws for positron production in laser–electron-beam collisions *Phys. Rev. A* **96** 022128
[13] Nerush E N, Kostyukov I Y, Fedotov A M, Narozhny N B, Elkina N V and Ruhl H 2011 Laser field absorption in self-generated electron-positron pair plasma *Phys. Rev. Lett.* **106** 035001
[14] Ridgers C P, Brady C S, Duclous R, Kirk J G, Bennett K, Arber T D, Robinson A P L and Bell A R 2012 Dense electron-positron plasmas and ultraintense γ rays from laser-irradiated solids *Phys. Rev. Lett.* **108** 165006
[15] Brady C S, Ridgers C P, Arber T D, Bell A R and Kirk J G 2012 Laser absorption in relativistically underdense plasmas by synchrotron radiation *Phys. Rev. Lett.* **109** 245006
[16] Ji L L, Pukhov A, Kostyukov I Y, Shen B F and Akli K 2014 Radiation-reaction trapping of electrons in extreme laser fields *Phys. Rev. Lett.* **112** 145003
[17] Stark D J, Toncian T and Arefiev A V 2016 Enhanced multi-MeV photon emission by a laser-driven electron beam in a self-generated magnetic field *Phys. Rev. Lett.* **116** 185003
[18] Wang W-M, Sheng Z-M, Gibbon P, Chen L-M, Li Y-T and Zhang J 2018 Collimated ultrabright gamma rays from electron wiggling along a petawatt laser-irradiated wire in the QED regime *Proc. Natl Acad. Sci.* **115** 9911–6
[19] Vranic M, Grismayer T, Meuren S, Fonseca R A and Silva L O 2019 Are we ready to transfer optical light to gamma-rays? *Phys. Plasmas* **26** 053103
[20] Yoon J W, Kim Y G, Choi I W, Sung J H, Lee H W, Lee S K and Nam C H 2021 Realization of laser intensity over 10^{23} W/cm^2 *Optica* **8** 630–5
[21] Pike O J, Mackenroth F, Hill E G and Rose S J 2014 A photon-photon collider in a vacuum hohlraum *Nat. Photon.* **8** 434–6
[22] Ribeyre X, d'Humières E, Jansen O, Jequier S, Tikhonchuk V T and Lobet M 2016 Pair creation in collision of γ-ray beams produced with high-intensity lasers *Phys. Rev. E* **93** 013201
[23] Yu J Q, Lu H Y, Takahashi T, Hu R H, Gong Z, Ma W J, Huang Y S, Chen C E and Yan X Q 2019 Creation of electron-positron pairs in photon-photon collisions driven by 10-PW laser pulses *Phys. Rev. Lett.* **122** 014802
[24] Wang T and Arefiev A 2020 Comment on 'creation of electron-positron pairs in photon-photon collisions driven by 10-PW laser pulses' *Phys. Rev. Lett.* **125** 079501

[25] He Y, Blackburn T G, Toncian T and Arefiev A V 2021 Dominance of γ-γ electron-positron pair creation in a plasma driven by high-intensity lasers *Commun. Phys.* **4** 139
[26] Song H-H, Wang W-M, Chen M and Sheng Z-M 2024 From linear to nonlinear Breit-Wheeler pair production in laser-solid interactions *Phys. Rev. E* **109** 035204
[27] Song H H, Wang W-M, Li Y-T, He Y, Tamburini M, Keitel C H and Sheng Z-M 2025 Detecting linear Breit-Wheeler signals with a laser-foil setup (arXiv:2501.06711 [physics.plasm-ph])
[28] Sugimoto K, He Y, Iwata N, Yeh I-L, Tangtartharakul K, Arefiev A and Sentoku Y 2023 Positron generation and acceleration in a self-organized photon collider enabled by an ultraintense laser pulse *Phys. Rev. Lett.* **131** 065102
[29] Li Y-F, Shaisultanov R, Chen Y-Y, Wan F, Hatsagortsyan K Z, Keitel C H and Li J-X 2020 Polarized ultrashort brilliant multi-GeV γ rays via single-shot laser-electron interaction *Phys. Rev. Lett.* **124** 014801
[30] Xue K, Dou Z-K, Wan F, Yu T-P, Wang W-M, Ren J-R, Zhao Q, Zhao Y-T, Xu Z-F and Li J-X 2020 Generation of highly-polarized high-energy brilliant γ-rays via laser-plasma interaction *Matter Radiat. Extremes* **5** 054402
[31] Song H-H, Wang W-M, Li Y-F, Li B-J, Li Y-T, Sheng Z-M, Chen L-M and Zhang J 2021 Spin and polarization effects on the nonlinear Breit–Wheeler pair production in laser-plasma interaction *New J. Phys.* **23** 075005
[32] Gong Z, Hatsagortsyan K Z and Keitel C H 2022 Deciphering *in situ* electron dynamics of ultrarelativistic plasma via polarization pattern of emitted γ-photons *Phys. Rev. Res.* **4** L022024
[33] Ginzburg I, Kotkin G, Panfil S, Serbo V and Telnov V 1984 Colliding γe and $\gamma\gamma$ beams based on single-pass e^-e^+ accelerators II. Polarization effects, monochromatization improvement *Nucl. Instrum. Methods Phys. Res.* **219** 5–24
[34] Zhao Q *et al* 2022 Signatures of linear Breit-Wheeler pair production in polarized $\gamma\gamma$ collisions *Phys. Rev. D* **105** L071902
[35] Zhao Q, Wu Y-X, Ababekri M, Li Z-P, Tang L and Li J-X 2023 Angle-dependent pair production in the polarized two-photon Breit-Wheeler process *Phys. Rev. D* **107** 096013
[36] Böttcher M 2014 The polarization dependence of $\gamma\gamma$ absorption—implications for γ-ray bursts and blazars *Astrophys. J.* **795** 35
[37] Baier V N, Katkov V M and Strakhovenko V M 1998 *Electromagnetic Processes at High Energies in Oriented Single Crystals* (World Scientific)
[38] Yokoya K 2011 User's manual of CAIN Version 2.42
[39] Cocke W and Holm D 1972 Lorentz transformation properties of the Stokes parameters *Nat. Phys. Sci.* **240** 161–2
[40] Jauch J M and Rohrlich F 1976 *The Theory of Photons and Electrons: the Relativistic Quantum Field Theory of Charged Particles With Spin One-Half* (Springer)
[41] Song H-H, Wang W-M and Li Y-T 2021 YUNIC: a multi-dimensional particle-in-cell code for laser-plasma interaction (arXiv:2104.00642 [physics.plasm-ph])
[42] Song H-H, Wang W-M and Li Y-T 2022 Dense polarized positrons from laser-irradiated foil targets in the QED regime *Phys. Rev. Lett.* **129** 035001
[43] Higginson D P, Link A and Schmidt A 2019 A pairwise nuclear fusion algorithm for weighted particle-in-cell plasma simulations *J. Comput. Phys.* **388** 439–53